

Effect of a Gaussian Random External Magnetic Field with Spatio-temporal Variation on Compensation in Ising Spin-1/2 Trilayered Square Ferrimagnets

Soham Chandra ^{*1}

¹*Department of Physics, Presidency University, 86/1 College Street, Kolkata -700 073, India*

Abstract

In this work, an extensive Metropolis Monte Carlo simulation is performed to investigate the steady-state magnetic and thermodynamic behaviour of a trilayered spin-1/2 Ising ferrimagnet with *square monolayers*, driven by external Gaussian random magnetic field with certain spatio-temporal variations. Such *thin* magnetic systems are interesting subjects for simulational studies as they exhibit *compensation phenomenon*. Here, two distinct theoretical atoms, A and B make up the *ABA* and *AAB* type of configurations. In *ABA*, A-atoms make up the surface layers and the mid-layer is composed up of B atoms. While, in *AAB*, A-atoms make up the top and mid-layer while the bottom layer is made up of B-atoms. The like atoms (A-A and B-B) ferromagnetically interact and the unlike atoms (A-B) interact antiferromagnetically. For the time-dependent external Gaussian random field, the mean is zero always and the standard deviation is increased to unity in steps. Depending upon the strength of the external Gaussian random field, the compensation and critical points shift and steady-state magnetic behaviours shift between different distinct type of ferrimagnetic behaviours. The compensation phenomenon even vanishes after crossing a finite threshold of standard deviation of the magnetic field for particular choices of the other controlling parameters. Like Chandra S.[Phys. Rev. E 104, 064126 (2021)], in the Hamiltonian parameter space of both the configurations islands of ferrimagnetic phase without compensation appear within the phase area with compensation of field-free case. The areas of such islands grow with increasing standard deviation of the external field, σ , obeying the scaling relation: $f(\sigma, A(\sigma)) = \sigma^{-b}A(\sigma)$ with $b_{ABA} = 1.913 \pm 0.137$ and $b_{AAB} = 1.625 \pm 0.066$.

Keywords: Spin-1/2 Ising square trilayer; Gaussian random external magnetic field; Spatio-temporal variation in field; Metropolis Monte Carlo simulation; Compensation temperature; No-compensation islands

*E-mail addresses: soham.rs@presiuniv.ac.in ; sohamc07@gmail.com

1 Introduction

Layered ferrimagnetic materials are interesting physical systems as their physical properties are often very different from the bulk. Though ferrimagnetism was discovered in 1948 [1], the experimental interest in ferrimagnetism has grown up rapidly with the discovery of thin film growth techniques, like, metalorganic chemical vapor deposition (MOCVD) [2], molecular-beam epitaxy (MBE) [3], pulsed laser deposition (PLD) [4], atomic layer deposition (ALD) [5]. Such experimental advancements have made growth of bilayered [6], trilayered [7], and multilayered [8,9] systems with desired characteristics a reality. Expectedly, theoretical and computational studies of layered magnets have also gained momentum. For a multilayered ferrimagnet, magnetizations of each of the monolayers may evolve differently with temperature. Combination of such different magnetic behaviours in specific cases, exhibit *compensation*. *Compensation point* for such layered magnets is a temperature lower than the critical temperature, where total magnetization vanishes but individual layers are magnetically ordered [1]. Compensation is not related to criticality of the system but the magnetic coercivity shows singularity at the compensation point [10,11] for some ferrimagnetic materials. Strong temperature dependence of the coercive field around the compensation point and compensation point about the room temperature, make such ferrimagnets useful for thermomagnetic recording [10].

Random Field Ising Model (RFIM) was developed by Larkin in 1970 [12]. This simple magnetic model shows many remarkable static and dynamic behaviours [13]. A few examples follow where Random field type phenomenology is experimentally observed in disordered systems:

(a) disorder-induced frustration and electronic transport in disordered insulators [14]; (b) structural phase transitions in random alloys [15]; (c) binary fluid mixtures in random porous media [16]. (d) systems near the metal-insulator transition [17,18]; (e) impurity pinned commensurate charge-density-wave systems [19]; and (f) melting of intercalates in layered compounds e.g. TiS_2 [20].

The simulational results and subsequent analyses in [21] and references therein explain how RFIM may describe various types of noises in magnets. The physical system of interest in this study is the trilayered spin-1/2 Ising ferrimagnet with square monolayers. The objective is to study the influence of the Gaussian random external magnetic field on the compensation phenomenon associated with such a trilayered ferrimagnet.

To probe compensation, numerical studies have been performed on equilibrium (field-free and in presence of static fields) properties of the layered Ising ferrimagnets on different lattice geometries [22–26]. But trilayered ferrimagnetic superlattices have not received that much of attention as bilayers and multilayers have. An advantage of using such a spin-1/2 Ising magnetic structure is, in field-free cases they show compensation effect [25](a), [25](b), [26](a), [26](b), [26](c), even without site-dilution or mixed-spin structures. So they are one of the simplest systems to exhibit compensation. In some of such systems, In [25](a), by MFA and EFA and in [25](b), by MC simulations with Wolff single cluster Algorithm, the authors have shown that under certain range of interaction strengths, different temperature dependencies of sublattice magnetisations cause the compensation point to appear in both ABA and AAB configurations. In [26](a), it was hinted that there may exist underlying mathematical relations between Inverse absolute of reduced residual magnetisation (IARRM for brevity, which may be considered as an interesting physical quantity for such kind of systems) and parameters of the trilayered, $s = 1/2$, Ising system and in [26](b), certain functional forms describing the systematics of compensation, are proposed for both the AAB and ABA configurations, which agree fairly well with accepted numerical results of [25](b). In [26](c), for a triangular trilayered spin-1/2 ferrimagnet, the magnetic description by traditional Monte Carlo Simulation is shown to be in very good agreement with the description provided by IARRM and Temperature interval between Critical and Compensation temperatures (TICCT). The results in [26](c) actually strengthens the conjecture proposed in [26](b). So the equilibrium studies are quite well established.

But real systems can't preserve the pristine nature and disorder is almost naturally expected for the description of any spin model. For the kind of the system used in this study, a few sources of time-dependent disorder are [26](d): (a) the number of interacting spins for a particular site may be changing with time (b) time varying interaction strength between pairs of spins (c) Even the nature of the spins (magnitude of spin, different magnetic atoms etc.) in the ordered structure may vary with time. It is naturally very hard to model such temporally varying disorders. In an attempt in this direction, in [27], the effect of uniform random external magnetic field, with spatio-temporal variations, on the trilayered spin-1/2 has been shown by a dynamic Hamiltonian. The ferrimagnetic Ising superlattice in this study is similar to the one used in [27]. Each site has spin value, $s = 1/2$, and contains three magnetic sub-layers on square lattice. Each alternate layer is exhaustively composed of by either A or B type of atoms. The magnetic atoms on the top and bottom layers do not interact. [Fig.-1]. The magnetic interaction between the like atoms (A-A and B-B) is ferromagnetic and between dislike atoms (A-B) is antiferromagnetic. Additionally to the cooperative interactions, the z -component of spins, S_i^z at each site couples with a Gaussian random external magnetic field, $h_i(t)$. At a particular site, this external field varies in time and at any time instant, the values of this field are different over the lattice sites.

The spins interact Ising-like, in-plane as well as inter-plane. The time dependent Hamiltonian for such a trilayered ferrimagnetic system is:

$$\begin{aligned}
 H(t) = & -J_{11} \sum_{\langle t, t' \rangle} S_t^z S_{t'}^z - J_{22} \sum_{\langle m, m' \rangle} S_m^z S_{m'}^z \\
 & - J_{33} \sum_{\langle b, b' \rangle} S_b^z S_{b'}^z - J_{12} \sum_{\langle t, m \rangle} S_t^z S_m^z - J_{23} \sum_{\langle m, b \rangle} S_m^z S_b^z \\
 & - \sum_i h_i(t) S_i^z
 \end{aligned} \tag{1}$$

$\langle t, t' \rangle$, $\langle m, m' \rangle$, $\langle b, b' \rangle$ are nearest-neighbor pairs in the top, mid and bottom layers respectively and $\langle t, m \rangle$, $\langle m, b \rangle$ are, respectively, pairs of nearest-neighbor sites in, top & mid and mid & bottom layers. The first three terms are for the intra-planar ferromagnetic interactions. The fourth and fifth terms are for the inter-planar nearest neighbour

interactions, between top and mid layers and mid and bottom layers, respectively. The sixth term denotes the *spin-field interaction term* of all the spins to the external Gaussian random magnetic field, at time instant t . Because of the interactions: $J_{AA} > 0$, $J_{BB} > 0$, and $J_{AB} < 0$. For an ABA type system, $J_{11} = J_{33} = J_{AA}$; $J_{22} = J_{BB}$ and $J_{12} = J_{23} = J_{AB}$. For an AAB type system, $J_{11} = J_{22} = J_{12} = J_{AA}$; $J_{33} = J_{BB}$ and $J_{23} = J_{AB}$.

Inspired by [27], in the current study, it will be shown by extensive Monte Carlo simulations, how the magnetic and thermodynamic behaviours of similar systems change in response to the external Gaussian random magnetic field with certain spatiotemporal variation. The objective of the present work is to establish, how a change in the nature of the continuous random external field effects the compensation phenomenon of the ABA and AAB type trilayered spin-1/2 Ising ferrimagnets. The plan of the paper follows. The simulational details are described in Section 2. Section 3 contains the numerical results and associated discussions. In Section 4, the summary of the work is presented.

2 Simulation Protocol

The Metropolis single spin-flip algorithm [30, 31] is employed for simulation of the system. The three square monolayers has L^2 sites with $L = 100$. The z -components of spin projections of nearest neighbours, S_i^z ($S_i^z = \pm 1$) contribute to the cooperative and spin-field interactions. At each site i , a *local, time-varying, Gaussian random field* h_i couples with each spin. In [25](b), Compensation temperature has been found to be practically constant for $L \geq 60$, for the systems of this study. So the system sizes in this study is statistically reliable for simulational investigation. For both the configurations, the systems are initiated at a high temperature paramagnetic phase, with randomly selected half of the total spin projections being "UP" (with $S_i^z = +1$) and the rest being "DOWN" (with $S_i^z = -1$) (Using 1 for 1/2 fixes up the energy scale). At a fixed temperature T , the spin flipping is governed by the Metropolis rate [32, 33], of Equation [2]:

$$P(S_i^z \rightarrow -S_i^z) = \min\{1, \exp(-\Delta E/k_B T)\} \quad (2)$$

where the associated change in internal energy in flipping the i -th spin projection from S_i^z to $-S_i^z$, is ΔE . Similar $3L^2$ individual, random single-spin updates constitute One Monte Carlo sweep (MCS) of the entire system. This *one MCS* is the unit of time in this study. *Periodic boundary conditions in-plane and Open boundary conditions along the vertical are employed.*

The systems are kept for 10^5 MCS at every temperature step. The last configuration at the previous *higher* temperature acts as the starting configuration at a new *lowere* temperature. In a field-free environment, for the first 5×10^4 MCS the system is allowed to *equilibrate* (the equilibration time is sufficient [Refer to Figure 5 and discussions therein]). After that the external field is switched on and kept switched on for the next 5×10^4 MCS. So for the systems, the *exposure time interval* in the field, δ is 5×10^4 . The temperatures are measured in units of J_{BB}/k_B . For each of the fixed standard deviation of the Gaussian random field, the system is observed for

seven equidistant values of J_{AA}/J_{BB} , from 0.04 to 1.0 with an interval of 0.16. For each fixed value of J_{AA}/J_{BB} , J_{AB}/J_{BB} is decreased from -0.04 to -1.0 with a step of -0.16 .

For any combination of J_{AA}/J_{BB} and J_{AB}/J_{BB} , and a fixed sd of the external field σ , the time averages of the following quantities are calculated after equilibration at any temperature, (T) in the following manner [27, 34]:

(1) Sublattice magnetisations are calculated at time instant say, t , by:

$$M_q(T, t) = \frac{1}{L^2} \sum_{x,y=1}^L (S_q^z(T, t))_{xy} \quad (3)$$

The time averaged sublattice magnetizations is calculated by:

$$\langle M_q(T) \rangle = \frac{1}{\delta} \int_{t_0}^{t_0+\delta} M_q(T, t) dt \quad (4)$$

where q is to be replaced by t, m or b for top, mid and bottom layers.

(2) The order parameter, O_T , for the trilayer at temperature, T is defined as:

$$O_T = \frac{1}{3} (\langle M_t(T) \rangle + \langle M_m(T) \rangle + \langle M_b(T) \rangle) \quad (5)$$

(3) Fluctuation of the order parameter, $\Delta O(T)$ at temperature, T as follows:

$$\Delta O(T) = \sqrt{\frac{1}{\delta} \int_{t_0}^{t_0+\delta} [M(T, t) - O_T]^2 dt} \quad (6)$$

where $M(T, t)$ is the total magnetisation of the whole system, at temperature, T , calculated at the (t -th time instant).

(4) The time averaged value of cooperative energy per site, $\langle E \rangle_T$, at temperature, T , is determined by:

$$\begin{aligned} \langle E \rangle_T^{ABA} &= \frac{-1}{3L^2\delta} \int_{t_0}^{t_0+\delta} dt [J_{AA} (\sum_{\langle t, t' \rangle} S_t^z S_{t'}^z \\ &+ \sum_{\langle b, b' \rangle} S_b^z S_{b'}^z) + J_{BB} \sum_{\langle m, m' \rangle} S_m^z S_{m'}^z \\ &+ J_{AB} (\sum_{\langle t, m \rangle} S_t^z S_m^z + \sum_{\langle m, b \rangle} S_m^z S_b^z)] \end{aligned} \quad (7)$$

and

$$\begin{aligned} \langle E \rangle_T^{AAB} &= \frac{-1}{3L^2\delta} \int_{t_0}^{t_0+\delta} dt [J_{AA} (\sum_{\langle t, t' \rangle} S_t^z S_{t'}^z \\ &+ \sum_{\langle m, m' \rangle} S_m^z S_{m'}^z \sum_{\langle t, m \rangle} S_t^z S_m^z) \\ &+ J_{BB} \sum_{\langle b, b' \rangle} S_b^z S_{b'}^z + J_{AB} \sum_{\langle m, b \rangle} S_m^z S_b^z] \end{aligned} \quad (8)$$

(5) The fluctuation of the cooperative energy per site at temperature, T , by:

$$\Delta E(T) = \sqrt{\frac{1}{\delta} \int_{t_0}^{t_0+\delta} [E(T, t) - \langle E \rangle_T]^2 dt} \quad (9)$$

where $E(T, t)$ is the instantaneous cooperative energy per site, for the system at time t and temperature, T , within the exposure interval, δ .

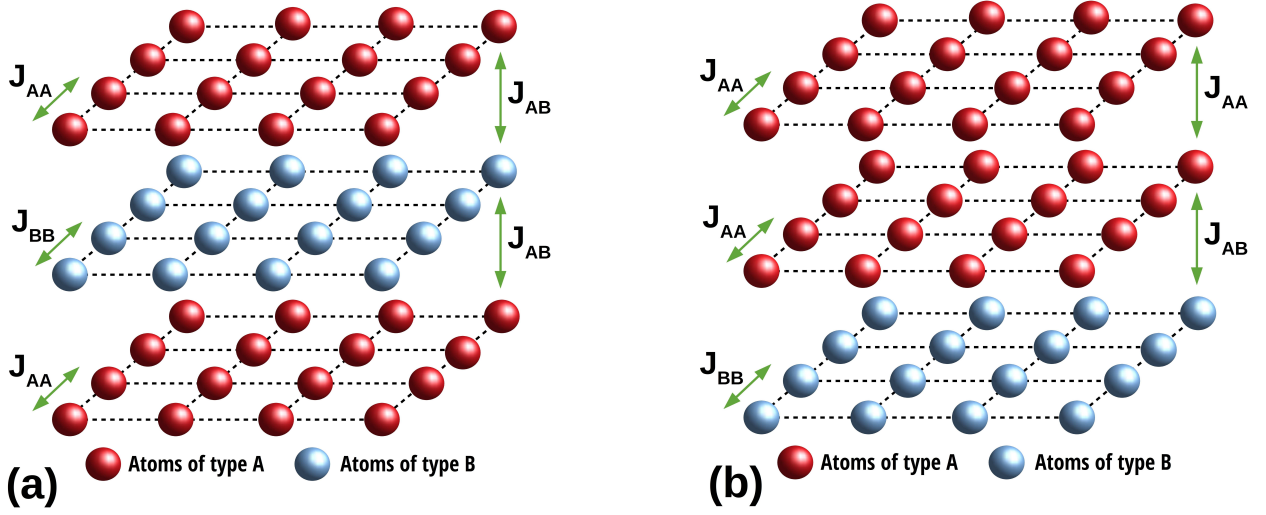


Figure 1: (Colour Online) Miniaturised versions ($3 \times 4 \times 4$) of (a) ABA and (b) AAB square trilayered ferrimagnet with two types of theoretical atoms, A and B . Each of the sublattices of the ferrimagnetic systems are formed on square lattice. The actual simulation is carried out on a system with $N_{sites} = 3 \times 100 \times 100$. Courtesy: [27]

At the pseudo-critical temperatures, the fluctuations peak. Around this temperature close range simulations were performed to narrow down the position of the *reported critical temperatures* with an accuracy of, $\Delta T_{crit} = 0.04$. Compensation temperature ($< T_{crit}$), where the total magnetisation again becomes zero, is determined by linear interpolation from the two neighbouring points across the zero of magnetization in the plots of order parameter vs. temperature [e.g. Figure 2(a)]. The Jackknife method [33] is used to provide an estimate of the errors with the magnetizations and fluctuations.

3 Results and discussions

3.1 Characteristics of the External field

The local, Gaussian random external magnetic field values $h_i(t)$ at any site, i at time instant t , is drawn from the following probability distribution:

$$P_{Gaussian}(h_i(t)) = \frac{1}{\sqrt{2\pi\sigma^2}} \exp\left(-\frac{h_i^2(t)}{2\sigma^2}\right) \quad (10)$$

with the standard deviation (sd) of the Gaussian distribution being, σ . To implement, Box-Muller algorithm [35] with the following formula is used to get a Gaussian distribution G_0 of sd, σ and zero mean:

$$G_0 = \sigma \sqrt{-2\ln(U_1)} \cos(2\pi U_2) \quad (11)$$

Here U_1 and U_2 are two uniform random distributions between $[0, 1]$.

A few additional characteristics are also added to the external field distribution [27]:

- (a) At different lattice sites, the values of the external field are uncorrelated at any time instant. Again at a lattice site, the values of the external field are uncorrelated for different time instants. So: $h_m(t)h_n(t') = a(t) \delta_{mn} \delta(t-t')$, where m, n are two different lattice sites and t, t' are two different time instants.

- (b) The following conditions are also satisfied:

- (i) After the field is switched ON, the bulk average of the Gaussian field at a time instant t , is zero:

$$\sum_m h_m(t) = 0$$

So,

$$\sum_{m,n} h_m(t)h_n(t)\delta_{mn} = 3L^2\sigma^2$$

- (ii) At the m -th site, the temporal mean of the local field over the exposure interval, δ , is zero:

$$\langle h_m(t) \rangle = \frac{1}{\delta} \int_{t_0}^{t_0+\delta} h_m(t) dt = 0.$$

At a few randomly chosen time instants within the exposure interval, the implementation of the desired field distribution is checked by the Cumulative Distribution Function (CDF) [28], the Kernel Density Estimate (KDE) [29] and the Histogram.

3.2 Thermodynamic Response

3.2.1 Magnetization versus temperature:

The thermodynamic response under the influence of uniform random magnetic field with spatio-temporal variation is established in [27]. For a few selective cases in Figure 2, we see exactly similar kind of a response. For a fixed standard deviation of the external field with characteristics of Section 3.1, the compensation and critical temperatures shift as we increase magnitude of any of the coupling strengths. According to [36–38], we can identify the nature of the magnetization curves as we increase the magnitude of either of the coupling strengths. In Figure 2 (a) for ABA configuration with $J_{AA}/J_{BB} = 0.20$ and $\sigma = 0.60$: for $J_{AB}/J_{BB} = -0.04$ we see a P-type; all the intermediate curves are of N-type and for $J_{AB}/J_{BB} = -1.00$ we see a R-type. In Figure 2 (b) with $J_{AB}/J_{BB} = -0.20$ and $\sigma =$

0.60: for $J_{AA}/J_{BB} = 0.04$ we see a P-type; the intermediate curves upto are of N-type and for $J_{AB}/J_{BB} = 1.00$ we see a Q-type. The L-type, within braces and not explicitly shown, would be encountered while moving from the first to the second set. For the most weak combination of coupling strengths, we witness the field-driven vanishing of compensation. In Figure 2 (c) for AAB configuration with $J_{AA}/J_{BB} = 0.20$ and $\sigma = 0.76$: for $J_{AB}/J_{BB} = -0.04$ we see a P-type; for $J_{AB}/J_{BB} = -0.20$ we see a L-type and all other curves are of N-type. In Figure 2 (d) for AAB configuration with $J_{AB}/J_{BB} = -0.20$ and $\sigma = 0.76$: for $J_{AA}/J_{BB} = 0.04$ we see a P-type; for $J_{AA}/J_{BB} = 0.20$ we see a L-type; the $J_{AA}/J_{BB} = 0.36, 0.52$ curves are of N-type; the $J_{AA}/J_{BB} = 0.68, 0.84$ curves are of Q-type and for $J_{AB}/J_{BB} = 1.00$ we see a P-type again. Again, for the AAB configuration as well, for the two most weak combinations of coupling strengths, we witness the field-driven vanishing of compensation.

Now we will focus on the effects of the external Gaussian random field has on the magnetic and thermodynamic behaviour. For any combination of coupling strengths, the compensation and critical temperatures decrease [Refer to Figure 3] with the increase in the value of standard deviation of the external Gaussian random field. As it was with the uniform random field [27], as we increase the randomness of the external Gaussian random field the decrement for the compensation temperatures is much more visible than the decrement of critical temperature, with or without compensation. The *field driven absence of compensation phenomenon* is also present in Figure 3(a) for ABA and Figures 3(e)&(f) for AAB configuration.

Like the uniform random external field, we can see and identify the nature of ferrimagnetic curves and field-driven transitions among them in Figure 3. According to the classification schemes of references [36–38]: **(A) For ABA**, in Figure 3(a), the magnetic response changes from type-N ($\sigma = 0, 0.20$) to type-L ($\sigma = 0.40$) to type-P ($\sigma = 0.60, 0.76, 1.00$); In Figure 3(b), for all the fields only type-N response is witnessed; and in Figures 3(c)&(d), we see only type-Q response for all the fields. **(B) For AAB**, in Figure 3(e), the transition happens from type-N ($\sigma = 0.00, 0.20$) to type-P ($\sigma = 0.40, 0.60, 0.76, 1.00$) via type-L; Similar transitions are witnessed in Figure 3(f); in Figure 3(g) & (h), all the magnetic responses are of type-Q.

3.2.2 Fluctuations versus temperature:

To better understand (a) the shifts of compensation and critical temperatures and (b) the reason behind the *field driven vanishing of compensation*, we will now observe both the fluctuations: fluctuation of the *order parameter* and fluctuation of the *cooperative energy per site*, as functions of temperature while sd of the external Gaussian random field acts as the parameter.

In Figure 4, where compensation happens, we witness a plateau with a smeared peak at the position of compensation for both the fluctuations of order parameter and energy. We clearly see the compensation and critical temperatures moving towards lower temperature values, with the increase in the sd of the Gaussian field. Even the smeared peaks at the low temperature segments flatten out as the sd is increased in steps, which signifies the van-

ishing of compensation. So we again witness a field-driven vanishing of compensation. At the lower parts of the temperature axis, the increase in both the fluctuations imply that magnetic ordering is gradually decreasing with the increase of the sd of the external field.

3.2.3 Magnetization versus time:

After the previous section showed us the decrease of magnetic ordering is associated with the field-driven vanishing of magnetisation, we will now observe how the sublattice magnetisations behave with time as the field is switched ON, at a suitably very low temperature $T = 0.01$. We have chosen three combinations of the coupling ratios: J_{AA}/J_{BB} and J_{AB}/J_{BB} [$\{(0.04, -0.20), (0.20, -0.20), (1.00, -0.52)\}$] for three values of sd [$\sigma = \{0.20, 0.60, 1.00\}$] of the external Gaussian random field for both the ABA and AAB configurations [Please refer to Figure 5]. At $T = 0.01$, till $t = 5 \times 10^4$ MCS, the Hamiltonian only has the associative part and the sublattice and total magnetisation of the system attains equilibrium. Just after $t = t_0 = 5 \times 10^4$ MCS, the external field is switched ON and the sublayer and total magnetisations *start to react*. As in the case with uniform random field [27], both the systems, ABA and AAB, reach the steady state very quickly. Conclusive features are unraveled in these cases.

Now, for the *ABA configuration*, we see in the top panel with $J_{AA}/J_{BB} = 0.04$ and $J_{AB}/J_{BB} = -0.20$, both the surface A-layers react magnetically for all the three sds of the external Gaussian field. The reason is, the per site associative energy is comparable to the spin-field energy. But the mid B-layer, with dominant in-plane coupling, remains in its equilibrium magnetic state. So it is evident that there is a competition between relevant energy scales: associative and spin-field. The similar inference is valid for the middle panel with the $\sigma = \{0.60, 1.00\}$ where per site spin-field energies are comparable to associative part of the Hamiltonian for the surface A-layers. The magnetization curves for the top and bottom layers overlap for the most of the times as they have identical magnetic neighborhood at low temperatures. Let's consider the case with $J_{AA}/J_{BB} = 0.04$, $J_{AB}/J_{BB} = -0.20$ and $\sigma = 1.00$ in the top panel. We see the randomisation of the surface layers lead to non-cancellation of the magnetization of the middle B-layer (that is why the total magnetisation remains positive, in the presence of the field), which causes the vanishing of compensation even in the lowest temperature limit.

For the *AAB configuration*, the influence of the bottom B-layer is limited to the middle A-layer (because of the nearest neighbour Ising interactions). So the top A-layer is much more affected by the external field than the middle A-layer. In top panel of Figure 5 for AAB with $\sigma = 0.60, 1.00$, when the spin-field energies per site dominates the cooperative energy per site of the A-layers, the A layers lose much of the magnetic ordering at such a low temperature and the top A-layer is almost randomised. So the combined magnetisation of A-layers is not enough to null the magnetisation of the bottom B-layer, leading to vanishing of compensation. Such a behaviour is qualitatively similar to what we have seen with uniform random field [27].

This is another example of *dynamic field-driven van-*

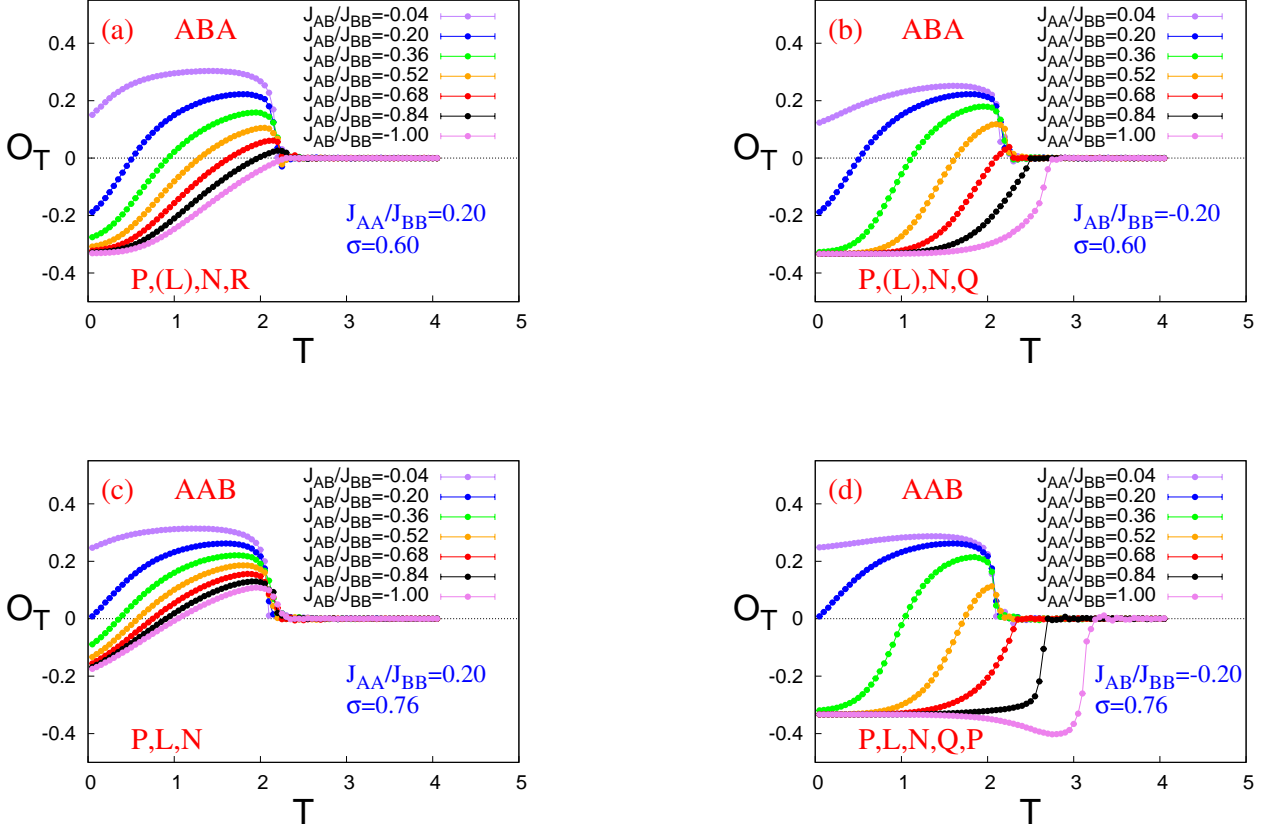


Figure 2: (Colour Online) Plots of Order parameter versus reduced temperature for: (a) ABA: $J_{AA}/J_{BB} = 0.20$ and variable J_{AB}/J_{BB} for $\sigma = 0.60$; (b) ABA: $J_{AB}/J_{BB} = -0.20$ and variable J_{AA}/J_{BB} for $\sigma = 0.60$; (c) AAB: $J_{AA}/J_{BB} = 0.20$ and variable J_{AB}/J_{BB} for $\sigma = 0.76$; (d) AAB: $J_{AB}/J_{BB} = -0.20$ and variable J_{AA}/J_{BB} for $\sigma = 0.76$. Shift of Compensation and Critical temperatures towards higher temperature end are witnessed with increase in any of the coupling ratios. The field-driven vanishing of compensation is witnessed for the weakest combination of coupling strengths.

ishing of compensation in the Ising spin-1/2 trilayers, driven by Gaussian random external field with spatiotemporal variation. The bottom panel with $J_{AA}/J_{BB} = 1.00$ and $J_{AB}/J_{BB} = -0.52$ for both the configurations supports that vanishing of compensation is a result of the competition between the associative and spin-field energies.

3.3 Phase Diagram and Scaling

In the Figure 6, a few examples of phase diagrams, under the influence of the Gaussian random external field, in the Hamiltonian parameter space, for both the configurations are shown. The features revealed here are qualitatively similar to the ones in [27]. For a given standard deviation of the field, compensation temperature merges with the critical temperature for higher values of J_{AA}/J_{BB} when $|J_{AB}/J_{BB}|$ is fixed or vice-versa, just like in the zero field case. In the diagrams, compensation is *present* (marked by P) within the orange areas and absence of compensation is marked by white areas (marked by A). The phase diagram is drawn following the procedures of zero-field cases [25, 26]. The extra feature is the enclave or islands with no-compensation within the phase area where parameters support compensation, like the one witnessed in the case with uniform random external field. In Figure 6, the

areas coloured in orange are where compensation is *present* (marked by P) and the area(s) in white are the regions where compensation is absent (marked by A). The qualitative features of the phase separation curves are same like that in the field-free cases. One of these curves divide the entire area of the parameter space into roughly two halves: one contains ferrimagnetic phases with compensation and the others contain ferrimagnetic phases without compensation. But the presence of the external Gaussian field [From $\sigma=0.2$, onwards], makes compensation disappear for a certain range of values of the coupling strengths [Refer to Figure 6]. In the phase diagrams, the range of values of relative coupling strengths for which compensation is absent are confined in areas within the region where compensation is present. These closed areas may be called No-Compensation Islands (NCI) after Ref. [27]. Similar to the case with uniform random magnetic field, the magnitude of areas of such an island also grows as the randomness of the external field increases.

In Figure 7, we see the plots of absolute area and rate of increase of absolute area versus the sd of the applied field. With reference to Figure 2, to get a closed curve for the boundary of the NCI, linear interpolation/extrapolation is employed between two adjacent points/at the boundary (coloured in blue). Next, the fractional area is obtained by

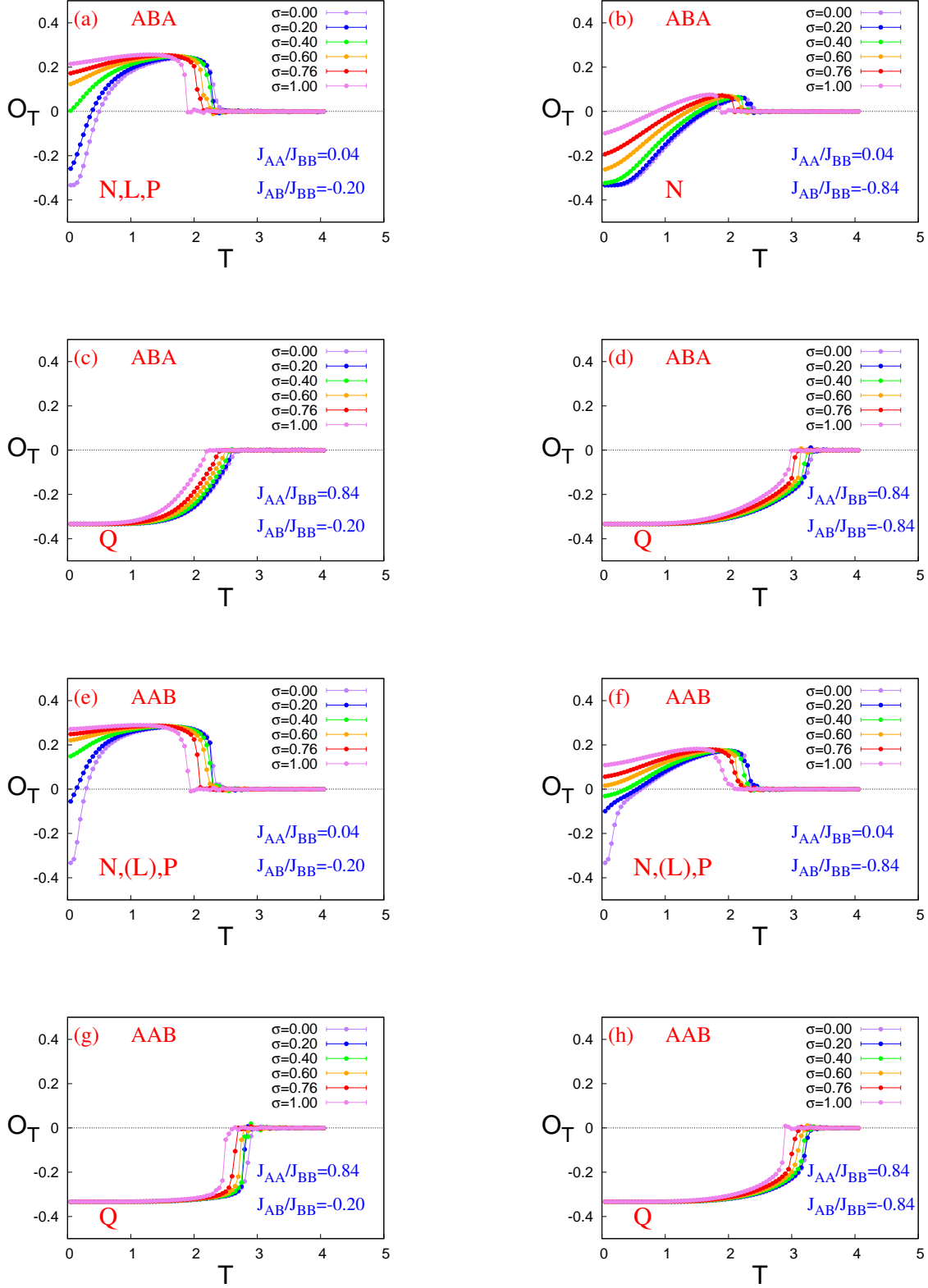


Figure 3: (Colour Online) Magnetic response of the trilayered system for a few selected cases with: (a)-(d) ABA and (e)-(h) AAB. The shift of both, the compensation (where it is present) and critical temperatures towards the low temperature ends and shift of the magnetic behaviours between N,L,P,Q etc. type of ferrimagnetism, with increase in standard deviation of the uniform random external magnetic field, are clearly visible in all these plots. The type L within brackets is explicitly not seen in the plots but encountered in-transition. In (a) and (e): we witness the field-driven vanishing of compensation from $\sigma = 0.20$ and upwards. Where, the errorbars are not visible, they are smaller than the area of the point-markers. All these plots are obtained for a system of $3 \times 100 \times 100$ sites.

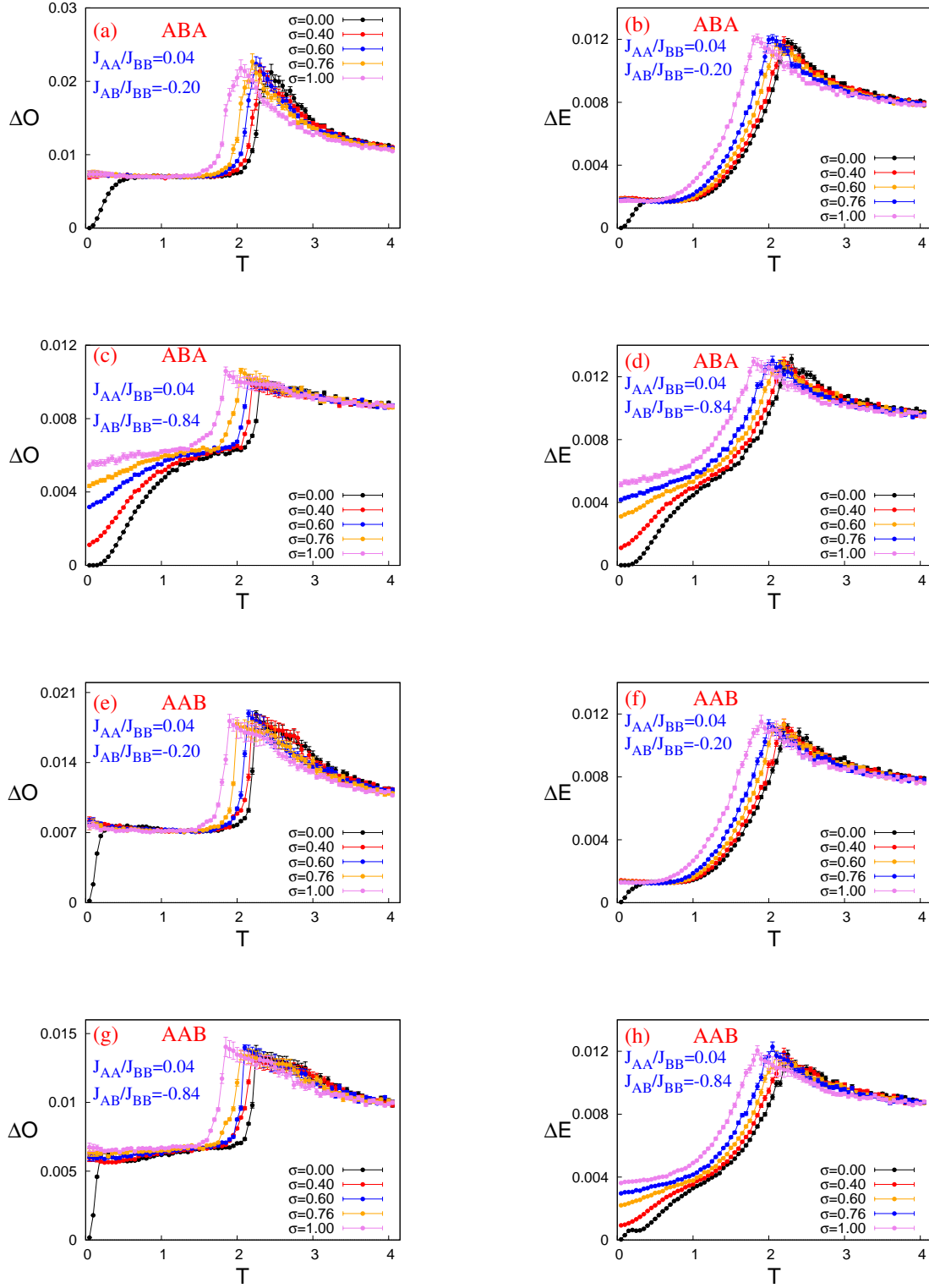


Figure 4: (Colour Online) Temperature dependence of Fluctuation of order parameter, ΔO and Fluctuation of cooperative energy per site, ΔE , for: ABA in (a)-(d) and AAB in (e)-(h) with $J_{AA}/J_{BB} = 0.04$ and $J_{AB}/J_{BB} = -0.04$ and with $J_{AA}/J_{BB} = 0.04$ and $J_{AB}/J_{BB} = -1.00$. Where, the errorbars are not visible, they are smaller than the area of the point-markers. All these plots are obtained for a system of $3 \times 100 \times 100$ sites. The nature of the curves prominently shows the shift of critical temperatures and even reason for absence of compensation can be understood from the low temperature segment of the curves.

Monte Carlo Integration [39]. Central difference formula is employed to find out the rate of increase of the area of NCIs to determine the nature of curve of the area of NCI vs. sd of the external field.

To analyse the nature of the curves of absolute area versus the sd, we note, the curve (in RED), comes out to be a mixture of *superlinear* and *sublinear* in nature, **for the ABA configuration**. From the BLUE curve of

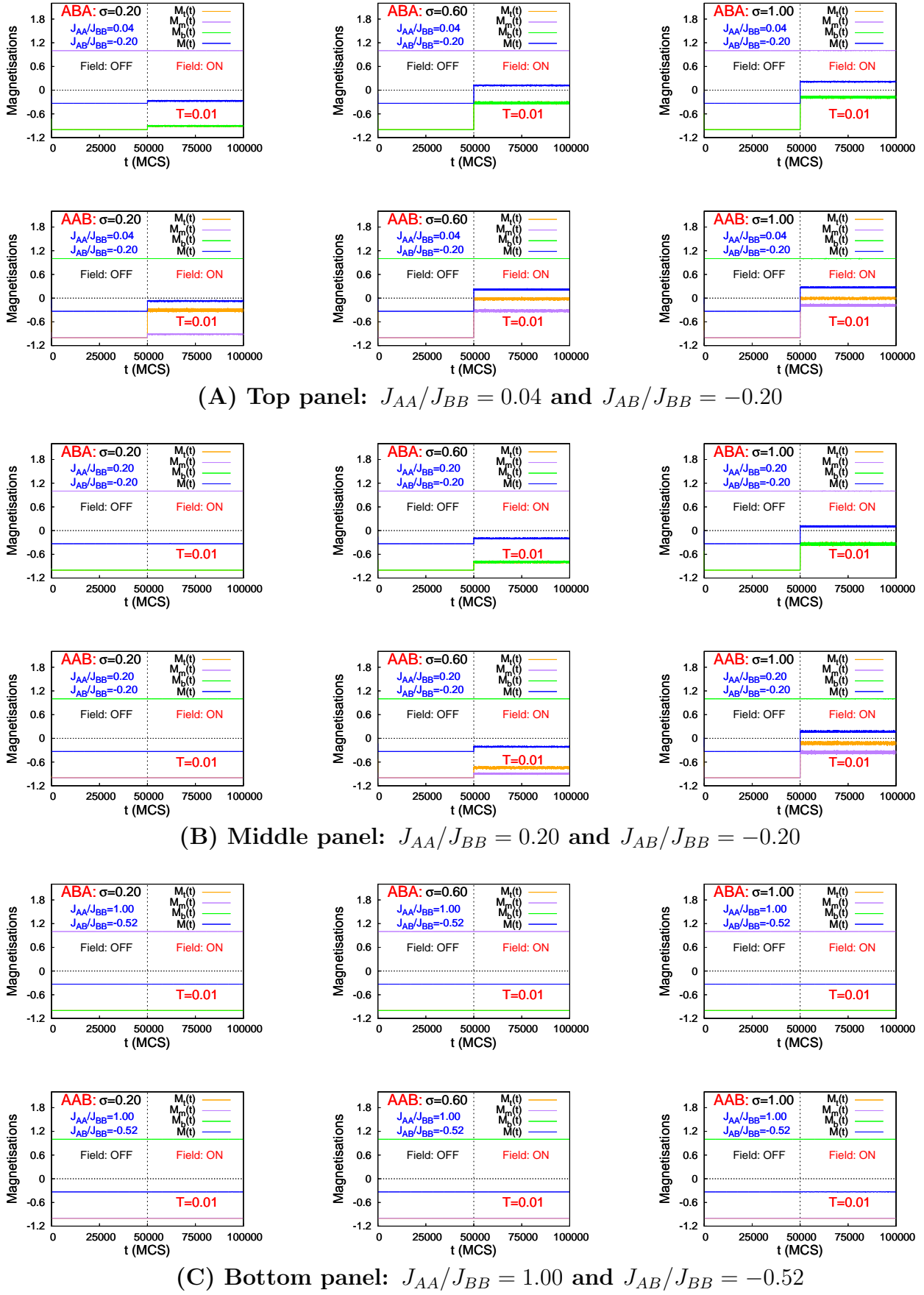


Figure 5: (Colour Online) Plots of Magnetisations for square monolayers (sublattices) and total magnetisation of the bulk versus time in MCS where $M_t(t)$: Magnetization of the top layer; $M_m(t)$: Magnetization of the mid layer; $M_b(t)$: Magnetization of the bottom layer are all functions of time, t , in units of MCS. The magnetisation curves for the surface layers (orange and green) of ABA configuration overlap for the most of the times.

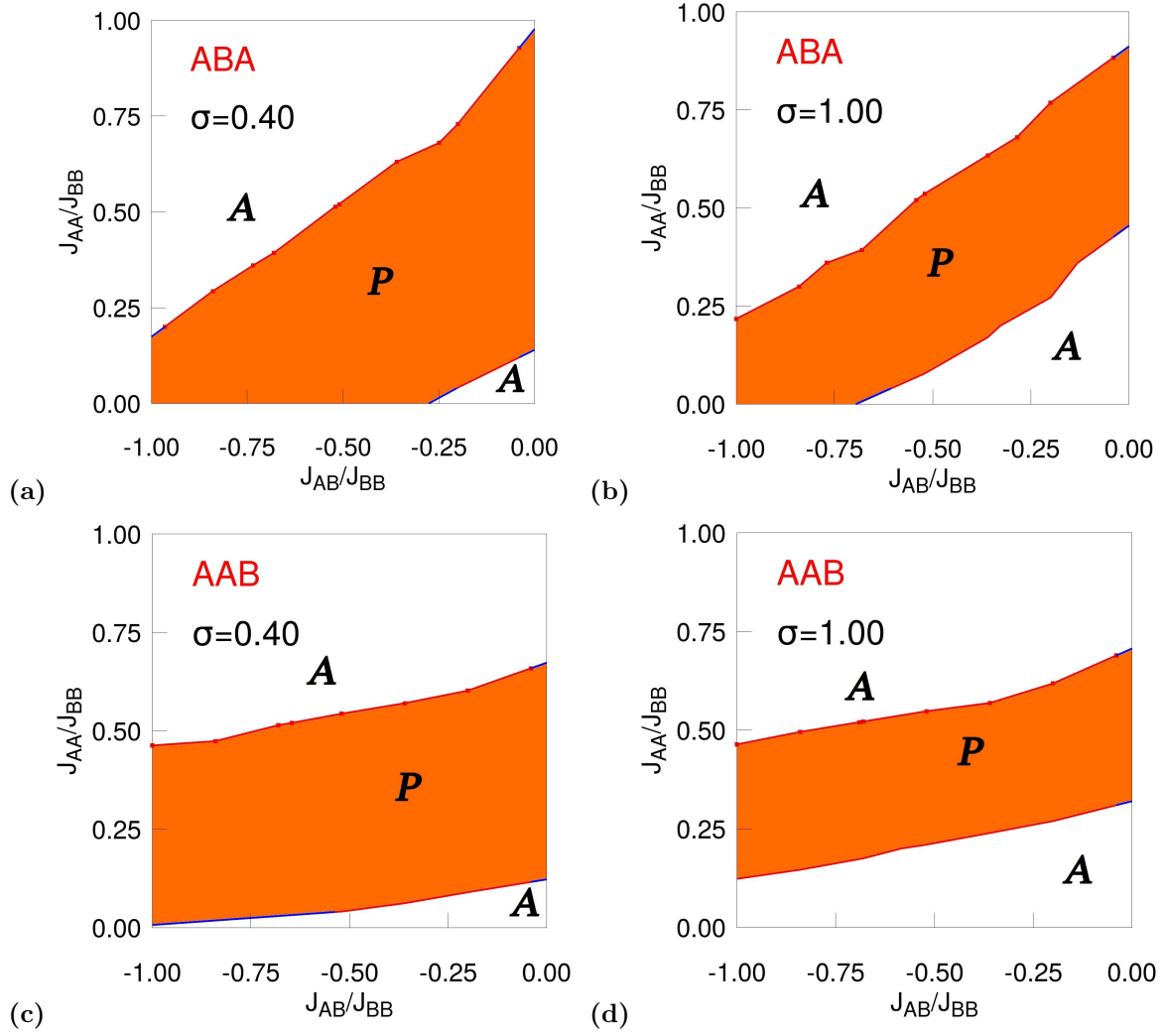


Figure 6: (Colour Online) Phase diagram for the: ABA trilayered ferrimagnetic system when: (a) $\sigma = 0.40$; (b) $\sigma = 1.00$ and AAB trilayered ferrimagnetic system when: (c) $\sigma = 0.40$; (d) $\sigma = 1.00$, in presence of the uniform random external magnetic field. A: Compensation is absent; P: Compensation is present. With increase in the standard deviation of the external field, the magnitude of the area of the no-compensation island have grown. The blue segment of the phase separation curves are obtained via linear extrapolation. All these plots are obtained for a system of $3 \times 100 \times 100$ sites. Where the errorbars are not visible, they are smaller than the point markers.

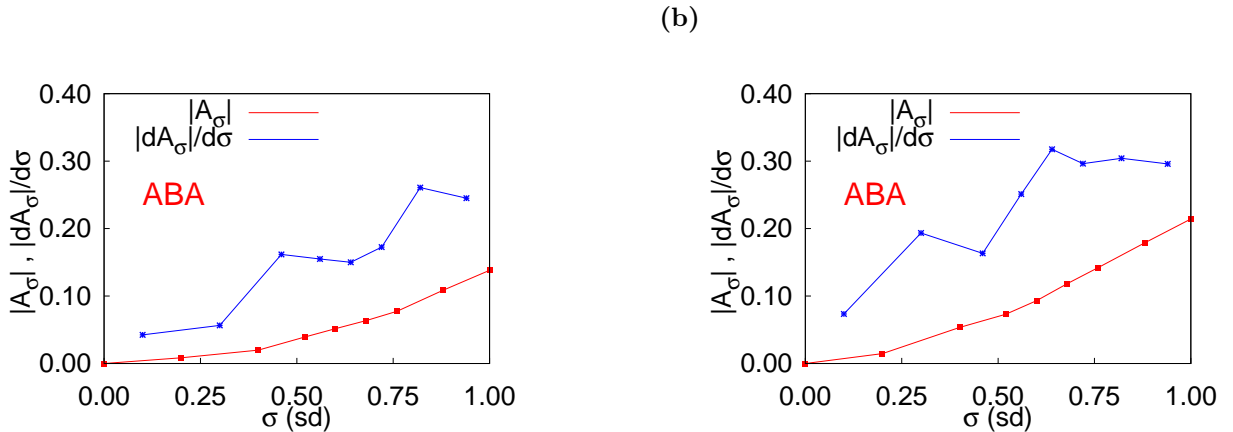


Figure 7: (Colour Online) Plots of: Magnitude of the area of the no-compensation islands versus standard deviation of the field (in RED) and the rate of increase in the magnitude of the area of the no-compensation islands versus standard deviation of the field (in BLUE) for (a) ABA and (b) AAB configurations for a system of $3 \times 100 \times 100$ sites.

slope versus sd of the field in Figure 7(a), in the vicinity of $\sigma = 0.60$ we find the curve follows a sublinear (almost linear) response. Again at and after $\sigma = 0.88$, the area changes in a prominent sublinear manner. At the low ran-

dom fields around $\sigma = 0.20$ and around moderately high randomness around $\sigma = 0.70$, the response is superlinear. **For the AAB configuration**, the area of NCIs increase superlinearly on average till $\sigma = 0.64$. After that the response becomes almost linear. Now the scaling between the magnitude of the area of NCIs and the sd of the field can be performed by the following scaling function [27]:

$$f(A(\sigma), \sigma) = \sigma^{-b} A(\sigma) \quad (12)$$

The scaling exponents come out to be: for ABA: $b_{ABA} = 1.913 \pm 0.137$ and for AAB: $b_{AAB} = 1.625 \pm 0.066$. A faithful estimate of error in the values of the exponents is obtained by the standard deviation among all the sets of data.

4 Summary and Conclusion

In this work, a Metropolis Monte Carlo study has been performed on the magnetic and thermodynamic responses of an Ising spin-1/2 square trilayered ferrimagnet, when subjected to a Gaussian Random external field. From [27], we have an idea about how such systems react under the influence of uniform random magnetic field. Now, from Section 3.2.1 we find that the magnetic response is qualitatively similar to the responses with uniform random field. Similar inference can be drawn for the thermodynamic behaviour of the suitably defined fluctuations of magnetization and associative energy [Refer to Section 3.2.2]. The effect of the time-dependent part of the Hamiltonian is established in Section 3.2.3. We observe that the systems react very quickly after switching ON the external field and the dynamics is governed by the competition between spin-field energies and associative energies, as it was the case in [27]. The phase diagrams in Figure 6, for both the ABA and AAB configurations, have similar kind of appearance with No-Compensation Islands engraved within the phase area with compensation.

*Now do these responses **quantitatively** differ?* A way to find out is to investigate the plot of the magnitude of area of NO-Compensation Islands versus the sd of the external field and finding out the scaling exponent according to the Equation 12. There we find a very good agreement, for the ABA configuration, with Uniform and Gaussian random external field. For the AAB configuration, we see the exponents overlap within the confidence interval of one-another. So the dynamic response of the trilayered Ising spin-1/2 ferrimagnetic systems, in this article, are quite similar under the influence of Gaussian random external magnetic field with spatiotemporal variations listed in Section 3.1 to the Uniform random external field [Please refer to [27]]. The exact nature of the external field distribution, for these two types of distributions, does not show a marked effect on the qualitative and quantitative features of such systems. In real magnetic systems impurities, compositional disorder, lattice dislocations etc. modify the Hamiltonian to a translationally non-invariant kind. Such a complexity, with Ising mechanics, may be described by a dynamic Hamiltonian such as Equation 1 with a time dependent part, where *the external field* is characterized by a probability distribution.

Acknowledgements

The author gratefully acknowledges financial assistance from the University Grants Commission, India in the form of Research Fellowship and extends his thanks to Dr. Tamaghna Maitra for suggestions, feedback and technical assistance.

References

1. Cullity B.D. and Graham C.D., Introduction to Magnetic Materials, second ed. (John Wiley & Sons, New Jersey, USA, 2008).
2. Stringfellow G.B., Organometallic Vapor-Phase Epitaxy: Theory and Practice (Academic Press, 1999).
3. Herman M.A. and Sitter H., Molecular Beam Epitaxy: Fundamentals and Current Status, Vol. 7 (Springer Science & Business Media, 2012).
4. Singh R.K. and Narayan J., Phys. Rev. B **41**, 8843 (1990).
5. George S.M., Chem. Rev. **110**, 111 (2010).
6. Stier M., and Nolting W., Phys. Rev. B **84**, 094417 (2011).
7. Leiner J., Lee H., Yoo T., Lee S., Kirby B. J., Tivakornsasithorn K., Liu X., Furdyna J. K., and Dobrowolska M., Phys. Rev. B **82**, 195205 (2010).
8. Sankowski P., and Kacmann P., Phys. Rev. B **71**, 201303(R) (2005).
9. Maitra T., Pradhan A., Mukherjee S., Mukherjee S., Nayak A., and Bhunia S., Phys. E **106**, 357 (2019).
10. Connell G., Allen R., and Mansuripur M., J. Appl. Phys. **53**, 7759 (1982).
11. Ostorero J., Escorne M., Pecheron-Guegan A., Soulette F., and Le Gall H., Journal of Applied Physics **75**, 6103 (1994).
12. Larkin A. I., Sov. J. Exp. Theo. Phys. **31**, 784 (1970)
13. Belanger D. P., and Young A. P., J. Magn. Magn. Mater. **100**, 272 (1991).
14. Efros A. L., and Shklovskii B. L., J. Phys. C **8**, L49 (1975).
15. Childress J. R., and Chien C. L., Phys. Rev. B **43**, 8089 (1991).
16. Maher J. V., Goldburg W. I., Pohlm D. W., and Lanz M., Phys. Rev. Lett. **53**, 60 (1984).
17. Pastor A. A., and Dobrosavljević V., Phys. Rev. Lett. **83**, 4642 (1999).
18. Kirkpatrick T. R., and Belitz D., Phys. Rev. Lett. **73**, 862 (1994).
19. (a) Fisher D. S., Phys. Rev. Lett. **50**, 1486 (1983).
(b) Fisher D. S., Phys. Rev. B **31**, 1396 (1985).
20. Suter R. M., Shafer M. W., Hornm P. M., and Dimon P., Phys. Rev. B **26**, 1495 (1982).
21. Sethna J. P., Dahmen K. A., and Perković O., in The Science of Hysteresis, Vol. II, pp. 107-179 (2006).
22. Oitmaa J., and Zheng W., Phys. A **328**, 185 (2003).
23. Lv D., Wang W., Liu J., Guo D., and Li S., J. Magn. Magn. Mater. **465**, 348 (2018).
24. Fadil Z. et al., Phys. B **564**, 104 (2019).
25. (a) Diaz I. J. L., and Branco N. S., Phys. B **529**, 73 (2017). (b) Diaz I. J. L., and Branco N. S., Phys. A **540**, 123014 (2019).
26. (a) Chandra S., and Acharyya M., AIP Conference Proceedings **2220**, 130037 (2020); DOI: 10.1063/5.0001865
(b) Chandra S., Eur. Phys. J. B **94(1)**, 13 (2021); DOI: 10.1140/epjb/s10051-020-00031-5
(c) Chandra S., J. Phys. Chem. Solids **156**, 110165 (2021); DOI: 10.1016/j.jpcs.2021.110165
27. Chandra S., Phys. Rev. E **104**, 064126 (2021); DOI: 10.1103/PhysRevE.104.064126
28. Deisenroth M. P., Aldo Faisal A., and Ong C. S., Mathematics for Machine Learning (Cambridge University Press, New York, 2020).
29. See, e.g., Rosenblatt M., Ann. Math. Statist. **27**, 832 (1956); Parzen E., Ann. Math. Statist. **33**, 1065 (1962).
30. Landau D. P. and Binder K., A Guide to Monte Carlo Simulations in Statistical Physics (Cambridge University Press, New York, 2000).
31. Binder K. and Heermann D. W., Monte Carlo Simulation in Statistical Physics (Springer, New York, 1997).
32. Metropolis N., Rosenbluth A. W., Rosenbluth M. N., Teller A. H., and Teller E., J. Chem. Phys. **21**, 1087 (1953).
33. Newman M. E. J. and Barkema G. T., Monte Carlo Methods in Statistical Physics (Oxford University Press, New York, 1999).
34. Robb D. T., Rikvold P. A., Berger A., and Novotny M. A., Phys. Rev. E **76**, 021124 (2007).
35. Box G. E. P. and Muller M. E., Ann. Math. Statist. **29(2)**, 610 (1958).
36. Néel M. L., Ann. de Phys. **12**, 137 (1948).
37. Chikazumi S., Physics of Ferromagnetism (Oxford University Press, Oxford, 1997).
38. Strečka J., Physica A **360**, 379 (2006).
39. See, e.g., Krauth W., Statistical Mechanics: Algorithms and Computations (Oxford University Press, New York, 2006).